Journal of Applied Polymer Science

Fabrication of Natural Cellulose Microspheres via Electrospraying from NaOH/Urea Aqueous System

Weibing Wu,[1] Jun Gu,[1] Guancheng Zhou,[1] Lei Zhang,[2] Murong Gong,[1] Hongqi Dai[1]

[1]Jiangsu Provincial Key Lab of Pulp & Paper Science & Technology, Nanjing Forestry University, Nanjing 210037, China
[2]School of Materials Science & Engineering, Nangjing University of Posts and Telecommunications, Nanjing 210046, China
Correspondence to: W. Wu (E-mail: wbwu@njfu.edu.cn)

ABSTRACT: Regenerated cellulose microspheres (RCM) with controllable sizes and architectures are prepared via electrospraying from environmental-friendly NaOH/Urea aqueous system. The particle size and shape of RCM is mainly dependent on the interplay among the electrical force, surface tension, and viscous force. Particle size can be reduced to a certain extent by increasing voltage and decreasing surface tension, electrode spacing, solution concentration, degree of polymerization, and flow rate. The deformation of droplets, which is peculiarly prone to occur for low viscosity and long electrode spacing, results in elongated spheres, tear-shaped particles, wedge-shaped particles, and banding shaped particles besides micorspheres. The sophericity and uniformity of particles generally become worse as a result of the deformation of droplets. RCM possess good porosity and large specific surface area after regeneration. © 2014 Wiley Periodicals, Inc. J. Appl. Polym. Sci. **2014**, *131*, 40656.

KEYWORDS: biomaterials; cellulose and other wood products; electrospinning

Received 11 October 2013; accepted 24 February 2014
DOI: 10.1002/app.40656

INTRODUCTION

The demand for the products made from renewable and sustainable resources are rapidly increasing recently. Cellulose, the most abundant and inexpensive nature polymers, is undoubtedly the most prospective renewable polymer resource available today.[1,2] Now, natural cellulose-based materials have been exploited from traditional cellulosic materials (forest products, paper, textiles, etc.) to new generation of cellulose-based products such as cellulose film, fiber, microspheres, nanoparticles, and so forth. Cellulose microspheres, which possess the advantages of dispersity, stability, porosity, and size controllability over natural cellulose particles, are widely used in chromatography,[3] separation engineering,[4] biomaterials,[5,6] targeting drug deliver and release,[7] and food.[8]

Several methods have been reported to prepare polymer microspheres, such as polymerization,[9,10] emulsification and curing,[3,11] coagulation and precipitation,[12] and spray drying.[13,14] However, above methods more or less have the limitations in the easiness of operation, controllability of particle size and shape, and environmental protection. Electrospraying, which can realize the liquid atomization by means of electrical forces, has opened new routes to micro- or nano-particle production, and micro- or nano-capsule formation.[15–17] Compared to mechanical atomizers and emulsification, electrospraying lowers the cost, cuts down the amount of organic solvents required, and reduces the environmental impact. In addition, the size of electrospray droplets can range from hundreds micrometers down to several tens of nanometer and the size distribution can usually be narrow.[18–20] Fabrication of polymer microspheres via electrospraying has drawn great attention in recent years. A variety of synthetic and natural polymers have been successfully formulated into microsphere form via electrosprayed molecular solutions.[21–24] However, electrospraying nature cellulose to generate cellulose microspheres is still a formidable challenge because the solvents to dissolve cellulose are relatively rare. From the point of view of economic and environment-friendly, the widely used no-devrivatization solvents such as N-methylmorpholine Noxide(NMNO),[25] lithium chloride/dimethylacetamide (DMAc),[26] ionic liquids,[27] ethylene diamine/salt[28] are still not the suitable solvents for dissolving and electrospraying cellulose. As an aqueous solvent, NaOH/Urea/H_2O is an ideal "green" solvent system for nature cellulose.[29,30] To our knowledge, no fabrication of nature cellulose microspheres via electrospraying from NaOH/urea aqueous system has been reported. In this article, we first prepared nature cellulose microspheres with different size and shape via electrospraying from NaOH/urea aqueous system. This work focuses on the modes of the liquid jet formation, jet breakup, droplet fission, droplet deformation, and droplet impact into coagulation bath and their influence on the physical form of microspheres. The observed formation of different sizes and shapes is interpreted

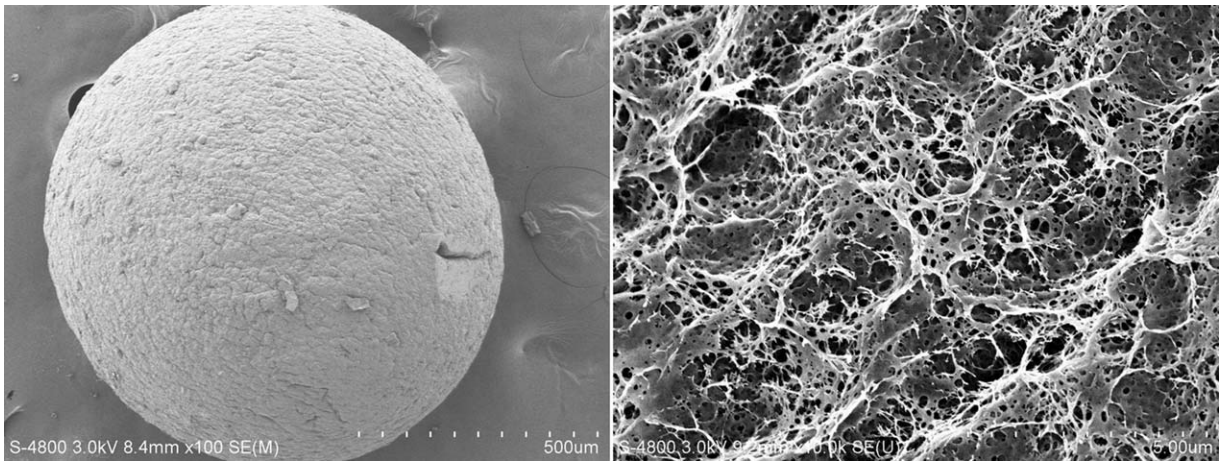

Figure 1. SEM images of typical RCM prepared from cellulose solution of NaOH/urea/H_2O.

on the basis of the interplay between electrical force, surface tension and viscous force. As structurally different particles are created and the use of organic reagents is avoided, the fabrication of natural cellulose microspheres via elecrospraying is a controllable and "green" technology.

EXPERIMENTAL

Materials

Cotton linter pulp board (Hubei Chemical Fiber Group Ltd., Hubei Xiangfan) was used as the raw material. Cellulose powders with different polymerization degree (DP) were obtained by milling the cotton linter. NaOH, urea, LiCl, dimethylacetamide (DMAc), sodium dodecyl benzene sulfonate (SDBS), H_2SO_4, Na_2SO_4, ethanol (Nanjing Chemical Reagent Co.), polyvinyl alcohol, ethyl cellulose (Sinopharm Chemical Reagent Co.) are all of analytical grade.

Preparation of Cellulose Solutions

Cellulose in NaOH/urea/H_2O: NaOH, urea and distilled water (NaOH: urea: H_2O = 8 wt %:12 wt %: 80 wt %) were mixed to obtain NaOH/urea aqueous solvent system. An appropriate amount of cellulose powders was added to the solvent. Then the mixture was stored in a refrigerator. After being precooled to −12.5°C, the mixture was vigorously stirred for 10 min. Subsequently, the cellulose solution was degassed through centrifugation at 3000 rpm for 5 min at room temperature. Cellulose solution containing surfactant was obtained through directly mixing SDBS with the original cellulose solution. Cellulose/PVA solution was prepared by mixing cellulose in NaOH/urea/H_2O and PVA in NaOH/urea/H_2O to form a homogeneous phase. All the cellulose solutions are preserved at 0–5°C.

Cellulose in DMAc/LiCl: Solvent of LiCl in DMAc was heated up to 110°C with oil bath, then cellulose powders were added and the mixture was stirred until transparent solution was obtained during the process of cooling.

Preparation of Regenerated Cellulose Microspheres (RCM)

The used electrospraying setup consists of a syringe positioned horizontally with its needle at high electric potential and a grounded metal collector. Cellulose solutions were fed mechanically using a micropump (LSP01-1A; Baoding Longer Precision Pump Co.) and the voltage was provided by a high voltage power supply (Dalian Ting Tong Technology Development Co.).

Cellulose solutions were loaded in the syringe and placed in the micropump. A flat copper mesh (approximately 10 × 10 cm) was placed 10–20 cm away from the tip of the needle (1.2 mm diameter) to collect the microspheres under various operating conditions. Electrospraying cellulose solutions was conducted over a wide range of electric field strengths by varying the voltage drop (0–15 kV) for a preset distance and using a number of different flow rates, <50 uL/min. Cellulose solutions of NaOH/urea/H_2O were solidified in the coagulation bath (Na_2SO_4: H_2SO_4: H_2O = 5 wt %: 5 wt %: 90 wt %) at room temperature. The coagulation bath for cellulose solution of DMAc/LiCl was deionized water. Microspheres from ethyl cellulose in ethanol were directly collected with slides and aluminum foil. The obtained RCM were washed five times with deionized water to remove the residual coagulation mixture.

Characterization

Solution viscosity was measured by rotary viscometer (NDJ-79). Measurement of surface tension was conducted on contact angle measuring system (KRUSS, America). The size and shape of RCM were analyzed using digital camera (IXUS220HS, Canon) and optical microscope (BX41, OLYMPUS). The surface morphology and porous structure were observed by scanning electron microscope (SEM; Hitachi, S-4800, Japan). Dimension analysis of microspheres was made using ImageJ software.

RESULTS AND DISCUSSION

Physical and Chemical Properties of Cellulose Microspheres

Morphology. Figure 1 shows the SEM images of typical RCM prepared from cellulose solution of NaOH/urea/H_2O. They are uniform in particle size and possess good sophericity. The pores with the average size in the range of 100–200 nm are distributed throughout the dried microspheres. The formation of porous structure can be attributed to the high moisture content (>80 wt %) and freeze drying method. Owing to the good porosity, the specific surface area of RCM is largely higher than that of traditional cellulose materials such as fiber and powder.

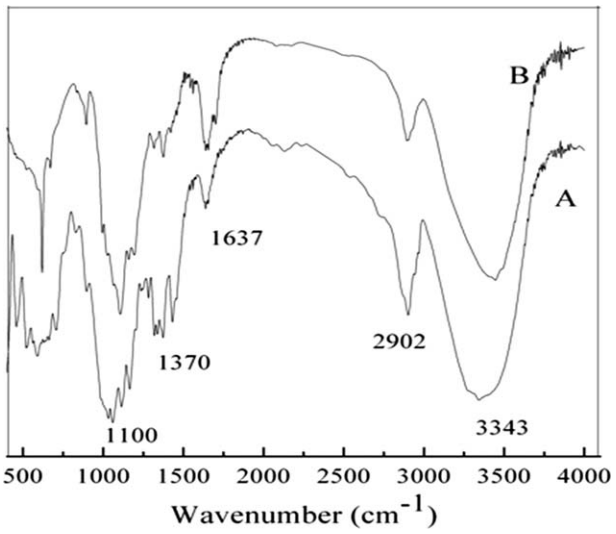

Figure 2. FTIR spectra of natural cellulose (A) and RCM (B).

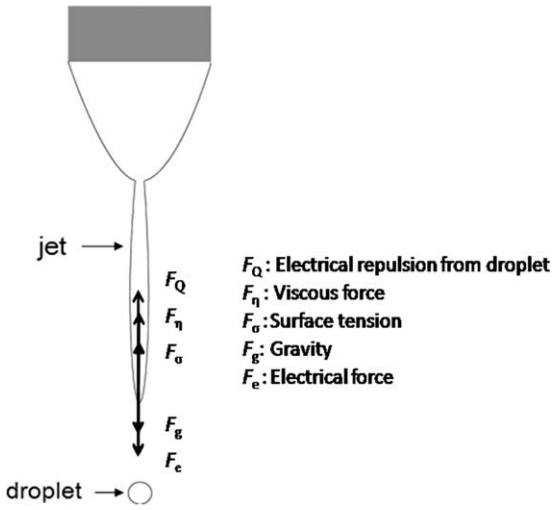

Figure 4. Schematic presentation of force analysis on the liquid jet in the cone-jet mode.

Chemical Properties. FTIR spectra of nature cellulose (A) and RCM (B) are illustrated in Figure 2. There is nearly no difference in the FTIR spectra between natural and regenerated cellulose. The peaks of both curves are consistent with the standard spectrum of cellulose, indicating that no chemical change of cellulose molecular structure occurs during the process of electrospraying. Compared to natural cellulose, the peak at 3343 cm^{-1} of RCM broadens and moves to higher wavelength. It means that the intermolecular hydrogen bond is enhanced after regeneration.[31] Figure 3 presents the XRD patterns of natural cellulose and RCM. Natural cellulose (B) gives diffraction peaks (2θ) at 15.1°, 16.6°, and 22.7°, which is consistent with the typical crystal structure of cellulose I. However, diffraction peaks of cellulose II at 12.3°, 20.1°, and 21.6° appear for RCM (A). Obviously, the crystal structure changes from cellulose I to cellulose II after regeneration.[32]

Influencing Factors on the Size and Shape of RCM

In the process of electrospraying, a sufficiently strong electric filed is build-up at the capillary outlet. Charged liquid by induction flows out from the nozzle and forms conically shaped meniscus called a Taylor cone.[17] A balance between the electrical force of repulsion between like charges at the surface, the surface tension force that oppose an increase in the gas–liquid interfacial area, electrical repulsion from droplet, viscous force, and gravity may be assumed to stabilize the Talyor cone at all points except near the apex, where the tangential forces because of electric field lines acting on the surface charges accelerate a jet of charged fluid toward the collector (Figure 4).[33,34] In this case, the liquid is elongated into a long, fine jet, which can be smooth and stable (cone-jet mode). During the dropping process, the formed liquid jet will undulate and break up into microspheres as a result of hydrodynamic instabilities caused by external vibrations and background noise that initiate the propagation of disturbance waves on the surface of the liquid jet.[35] The classical theory predicts the cylinder breaks up into homogeneously sized elongated or spherical droplets, which further retract back to form spheres of equal size. The characteristic size of the droplets formed from a given jet subjected to a particular electrification is directly related to the wavelength of the disturbance.[36] In our electrospraying experiments, almost monodisperse RCM were obtained under the right conditions [Figure 5(A)]. However, in other cases, as the liquid jet flows from the necks to the bulges, the deformation of the surface usually induces different fission points.[35] The bulge area breaks up into large droplets, accompanied by smaller satellite droplets originating from the neck areas, consistent with the presence of the small microspheres observed, as illustrated schematically in Figure 5(B). By selecting the surface tension, electrostatic voltage, viscosity, flow rate, concentration, electrode spacing, and electrical conductivity, one can control the fission mode of liquid jet to a certain extent, subsequently, govern the size and shape of the resulting particles.[37] This is indeed observed in Table I.

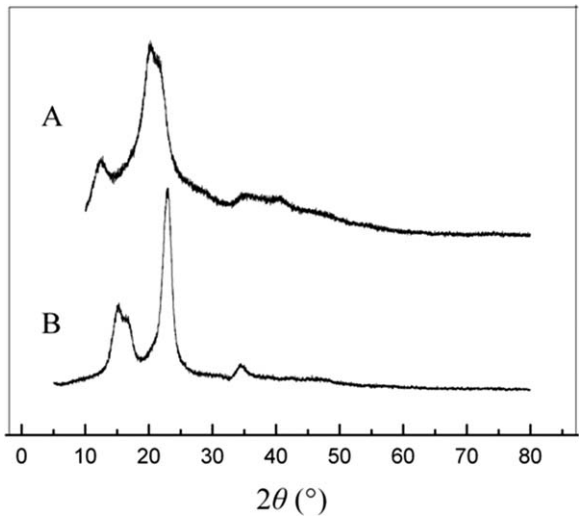

Figure 3. XRD analysis of RCM (A) and natural cellulose (B).

Electrical Force. Electrical force, the main driving force for the breakup of liquid jet, is related to voltage and electrode spacing. Average diameter (D_{av}) of RCM reduces significantly from

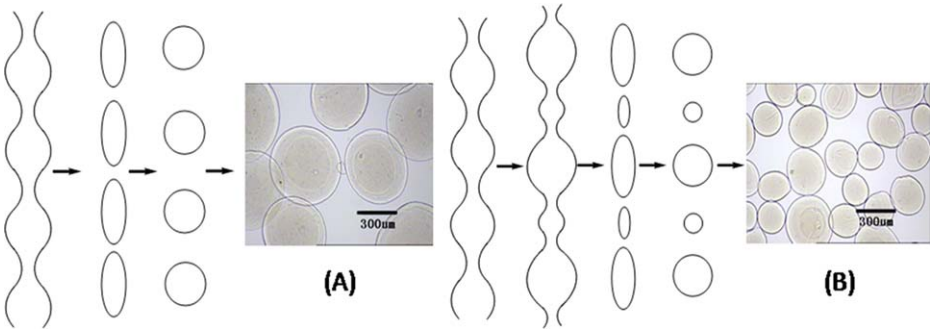

Figure 5. Possible mechanisms for the undulate and fission of droplets and the morphology of microspheres. [Color figure can be viewed in the online issue, which is available at wileyonlinelibrary.com.]

2.5 mm to 885 μm with an increase in the voltage in the range of 0–10 kV. It is consistent with the conclusion that increasing charge density on the droplets at high voltage promotes the breakup of liquid jet into smaller droplets.[34] The particle size decreases by rather modest amounts but coefficient variation (CV) increases obviously when the voltage further increases. For example, D_{av} of RCM_{V15} is merely reduced to 734 μm but CV reaches to 19.1%. In our experiments, stable cone-jet mode is formed around 10 kV, further increase in the voltage (>15 kV) gradually destroy the stability of jetting and finally causes irregular multijet mode. In fact, multijet mode results in the coexistence of small and large microspheres, which directly leads to the limited decrease in D_{av} and rapid increase in CV.[33] As electrode spacing increases from 10 to 25 cm, D_{av} and CV increase from 222 to 308 μm and 29.0 to 48.7%, respectively. When the electrode spacing is <10 cm, there are lots of nonuniform ellipsoids observed. The appearance of ellipsoids may be ascribed to the incomplete retraction of deformed droplets before dropping into coagulation bath. On the contrary, insufficient breakup which causes large particle size occurs when the electrode spacing exceeds 20 cm. The bad sophericity may be attributed to the intense impact into coagulation bath after the acceleration of droplets in a long distance. Optimized sophericity and the lowest CV are obtained for the electrode spacing of 15 cm, at

Table I. Details of RCM

Sample[a]	DP	*C* (wt %)	η (mPa s)	*V* (kv)	*Q* (uL/min)	*D* (cm)	Shape[b]	D_{av} (μm)	CV (%)
RCM_{V0}	500	3	321	0	10	15	S	2503	6.6
RCM_{V5}	500	3	321	5	10	15	S	1156	11.0
RCM_{V10}	500	3	321	10	10	15	S	885	11.4
RCM_{V15}	500	3	321	15	10	15	S	734	19.1
RCM_{Q10}	361	2	65	10	10	15	S	237	21.7
RCM_{Q20}	361	2	65	10	20	15	S, So	322	17.1
RCM_{Q30}	361	2	65	10	30	15	S, IS	371	16.1
RCM_{Q40}	361	2	65	10	40	15	IS, WS	400	16.2
RCM_{D10}	361	2	65	10	10	10	S, So	222	29.0
RCM_{D15}	361	2	65	10	10	15	S	237	21.7
RCM_{D20}	361	2	65	10	10	20	WS, TS	304	31.5
RCM_{D25}	361	2	65	10	10	25	WS, TS, IS	308	48.7
$RCM_{C0.5}$	500	0.5	6.2	10	10	15	BS	-	-
RCM_{C1}	500	1	12	10	10	15	TS, So, WS	152	17.8
RCM_{C2}	500	2	115	10	10	15	S	821	12.3
RCM_{C3}	500	3	195	10	10	15	S	885	11.4
RCM_{DP404}	404	2	84	10	10	15	S	561	18.7
RCM_{DP361}	361	2	65	10	10	15	S	237	21.7
RCM_{DP238}	238	2	32	10	10	15	S, WS	170	34.8
RCM_{DP151}	151	2	12	10	10	15	BS	-	-

[a] η, solution viscosity; D_{av}, the average diameter of RCM; CV, coefficient of variation; RCM_V, RCM_Q, RCM_D, RCM_C, and RCM_{DP} are RCM under different voltages (*V*), flow rates (*Q*), electrode spacing (*D*), concentrations (*C*), and degree of polymerization (DP), respectively.
[b] S, sphericity; So, spheroidicity; IS, irregular sphericity; TS, tear shape; WS, wedge shape; BS, banding shape.

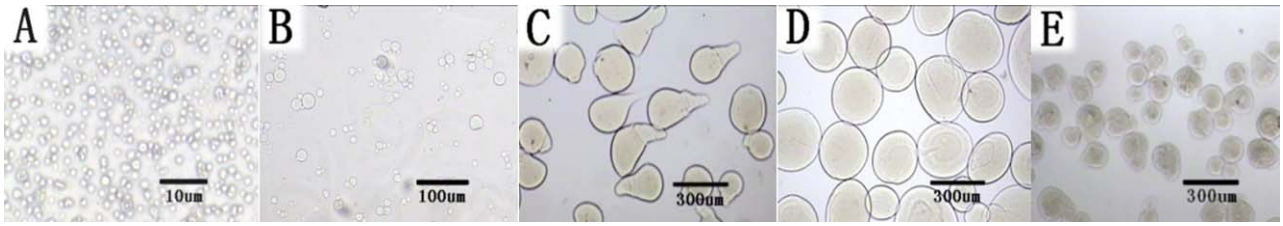

Figure 6. Optical images of RCM from different cellulose solutions [A: Ethyl cellulose in ethanol; B: Cellulose in LiCl/DMAc; C: Cellulose in NaOH/urea/H_2O; D: Cellulose in NaOH/urea/H_2O mixed with SDBS (1 wt % base on cellulose); E: Cellulose/PVA (cellulose: PVA = 50 wt %: 50 wt %) in NaOH/urea/H_2O]. [Color figure can be viewed in the online issue, which is available at wileyonlinelibrary.com.]

which the retraction of droplets is complete while the impact of acceleration is limited.

Surface Tension. Surface tension is an important factor that influences the jetting and breakup during the process of electrospraying.[38] In order to study its influence on the size and shape of RCM, three different cellulose solutions including ethyl cellulose in ethanol, cellulose in LiCl/DMAc and cellulose in NaOH/urea/H_2O were selected to prepare RCM via electrospraying. Figure 6 presents the optical images of RCM from different cellulose solutions. It is noted that D_{av} rapidly decreases when the solvent system is changed from NaOH/urea/H_2O to LiCl/DMAc and further to ethanol (RCMC, RCM_{CL}, and RCM_{EC}). As other parameters including voltage, flow rate, and electrode spacing are set to the same value and the influence of electrical repulsion from droplet and gravity is negligible,[17] the difference in D_{av} can be mainly ascribed to the surface tension and conductivity of solutions. As seen from Table II, D_{av} increases with an increase in both surface tension and conductivity. It is known that increasing solution conductivity can increase the surface charge accumulation of droplets. Hence, the fission of sprayed droplets will be enhanced as a result of the increasing electrostatic repulsive force. It will lead to the reduction of D_{av}. Surface tension is a kind of force that tends to maintain the smallest superficial area and the lowest surface energy, and the increase in surface tension will hinder the fission of droplets and result in large particle size. When the solution is changed from organic solvent to aqueous solvent, the surface tension gradually increases and RCM with increasing D_{av} are resulted. Actually, Smith noticed that a liquid can hardly be atomised by electrostatic forces when its surface tension is higher than 50 mN/m.[39] Comparing the final trend of D_{av} under the competition of surface tension and solution conductivity, it can be concluded that the former is more crucial than the latter in deciding D_{av} of RCM during the electrospraying process. Related report[33,40] that the effect of solution conductivity on D_{av} is limited further supports our viewpoint. So the production of large RCM with D_{av} more than 100 μm is reasonable.

Based on the conclusion that D_{av} can be generally tuned by changing the surface tension, we tried two ways to investigate the feasibility of controlling D_{av} for NaOH/urea aqueous system. Two kinds of cellulose solutions with reduced surface tension are designed as follows: one is cellulose/PVA in NaOH/urea/H_2O; the other is cellulose in NaOH/urea/H_2O mixed with surfactant, as seen in Table II. For the cellulose solution containing PVA, the surface tension decreases from 72.7 to 45.8 mN/m and D_{av} of RCM_{CP} is reduced by 43% compared to that of RCM_C. It is noted that the degree of the decrease in D_{av} is not as much as that of RCM_{CL} and RCM_{EC}. For organic solvents such as DMAc and ethanol, the existing solvent evaporation not only causes the retraction of droplets but also promotes the Coulomb fission of large droplets into smaller droplets owing to the increasing surface charge density. However, the process of breakup cannot continue for NaOH/urea aqueous system since there is no solvent evaporation and no increase in the surface charge density. It may be the main reason for the limited decrease in the particle size of RCM_{CP} compared to the notable decrease in the surface tension for the aqueous solvent system. For the cellulose solution mixed with surfactant (0.5 wt % SDBS base on cellulose), surface tension is reduced from 72.7 to 41.3 mN/m, which is lower than the 45.8 mN/m of cellulose solution containing PVA. However, D_{av} of $RCM_{CS0.5}$ only decreases to 203 μm, which is much higher than the 130 μm of RCM_{CP}. No essential change of D_{av} is observed when the addition of surfactant is increased to 1 wt % (RCM_{CS1}, 185 μm) and 2 wt % (RCM_{CS2}, 182 μm). Considering that cellulose solution mixed with surfactant is not a homogeneous phase system, we believe that there are not enough surfactant molecules covering the droplet surface as the fission of droplets continue. As a

Table II. Surface Tension of Cellulose Solutions and Corresponding Particle Sizes of RCM

Sample[a]	RCM_{EC}	RCM_{CL}	RCM_C	RCM_{CP}	$RCM_{CS0.5}$	RCM_{CS1}	RCM_{CS2}
σ (mN/m)	20.5	36.6	72.7	45.8	41.3	29.2	28.4
K (ms/cm)	0.045	3.41	372	368	361	356	355
D_{av} (μm)	2.5	21	237	130	203	185	182

σ, surface tension; K, solution conductivity.
[a] RCM_{EC}, RCM_{CL}, RCM_C, RCM_{CP}, $RCM_{CS0.5}$, and RCM_{CS1} represent RCM from ethyl cellulose in ethanol, cellulose in LiCl/DMAc, cellulose in NaOH/urea/H_2O, cellulose/PVA (cellulose: PVA = 50 wt %: 50 wt %) in NaOH/urea/H_2O, cellulose in NaOH/urea/H_2O mixed with 0.5 wt % SDBS (base on cellulose), cellulose in NaOH/urea/H_2O mixed with 1 wt % SDBS, and cellulose in NaOH/urea/H_2O mixed with 2 wt %, SDBS respectively.

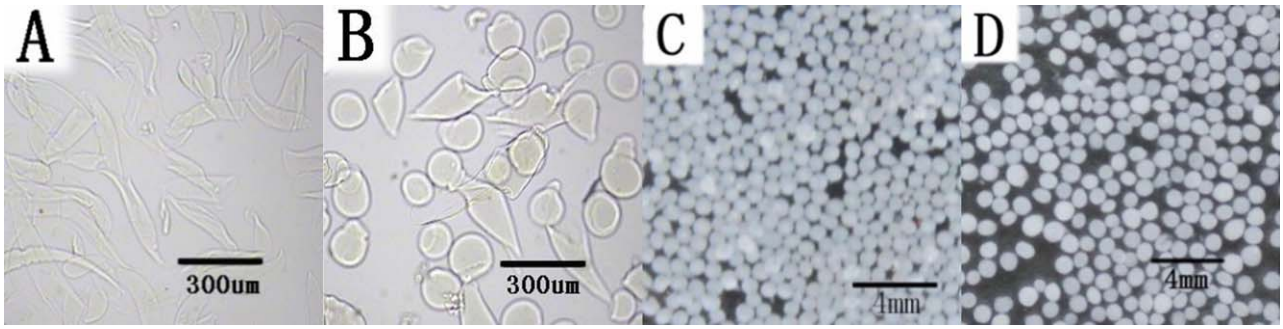

Figure 7. Optical images of RCM from different cellulose solutions [A: Ethyl cellulose in ethanol; B: Cellulose in LiCl/DMAc; C: Cellulose in NaOH/urea/H_2O; D: Cellulose in NaOH/urea/H_2O mixed with SDBS (1 wt % base on cellulose); E: Cellulose/PVA (cellulose: PVA = 50 wt %: 50 wt %) in NaOH/urea/H_2O]. [Color figure can be viewed in the online issue, which is available at wileyonlinelibrary.com.]

result, the real surface tension of droplets after breakup could be higher than that measured by drop weight method. The heterogeneous distribution of surfactant may also cause the variation of surface tension and asymmetrical retraction of droplets, which further result in tear-shaped particles and irregular particles with tails besides microspheres [as seen in Figure 6(C)].

Viscous Force. Viscous force, the expression of intermolecular friction and entanglement, is related to the solution viscosity. Typically, the viscosity of polymer solution depends upon the solution concentration and molecular weight.[41,42] As seen in Table I, there is an increase in the viscosity with an increase in both concentration and DP. Figures 7 and 8 present the optical images of RCM from cellulose solutions with different concentrations and DP. At the concentration of 0.5 wt %, there are no microspheres but banding-shaped particles observed. Ellipsoid, tear-shaped, and wedge-shaped particles are obtained with the concentration of 1 wt %. Uniform microspheres with no obvious defects appear when the concentration reaches to 2 and 3 wt %. The effect of DP on the particle size and shape is similar to that of concentration.

The phenomenon of the deformation of spherical droplets into other shapes has been observed and reported.[43,44] It can be explained qualitatively as follows. Generally, droplets will retract back to form spherical microspheres under the action of surface tension. However, a charged droplet is typically elongated into an ellipsoid, banding shape or q-tips in the electrical field. As the fluid flow proceeds, the q-tips eventually break in half to form tear-shaped and wedge-shaped droplets. There are three possible outcomes for these intermediate droplets: First, retract back to a spherical shape; Second, remain unchanged and be solidified in the coagulation bath; the last, repeat the process of breakup. Figure 9 outlines the different stages in the fission of an elongated droplet. Viscous force is a force that hinders the deformation and fission of the droplets, so it is a key factor that decides the particle shape and architecture. At high viscosity, the deformation and fission of spherical droplets is largely limited because of increasing viscous force. As a result, the droplets stay unaffected and are frozen into their final structure of relatively large particle size and good sophericity, as seen for RCM_C and RCM_{DP} series in Table I. When the viscosity further increases up to 80 mPa s in our experiment, electrical force is not strong enough to overcome viscous force to realize jet mode. Under this circumstance, dripping mode with insufficient fission of droplets forms and large RCM are produced. The formation of banding-shaped particles can be attributed to the elasticity of cellulose solution at low viscosity. Instead of retracting back to a spherical shape, the elongated droplet will be elongated further as a result of weak viscous force.

Flow Rate. Flow rate, which influences the surface charge density and distribution, is a crucial factor that decides the particle size and shape. When flow rate increases from 10 to 40 μL/min, D_{av} gradually increases from 237 to 400 μm and the sophericity grows bad (Table I, RCM_Q series). Increasing flow rate means the reduction of charge density on the surface of droplets. As a result, the breakup of liquid jet and droplets is limited and D_{av} increases. At high flow rate, the charge may not be able to disperse well on the whole droplet. Thus, the local limit of charge distribution on the surface causes irregular jet and hence creates particles with bad sophericity. Another reason of the bad

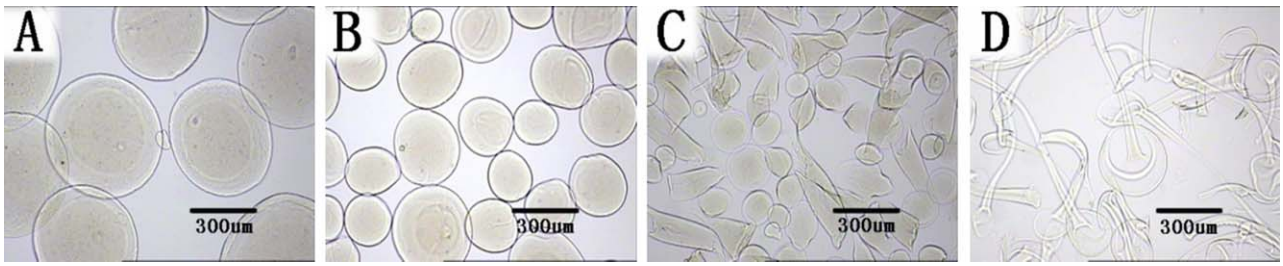

Figure 8. Optical images of RCM from cellulos solutions with different DP (A: RCM_{DP404}; B: RCM_{DP361}; C: RCM_{DP238}; D: RCM_{DP151}). [Color figure can be viewed in the online issue, which is available at wileyonlinelibrary.com.]

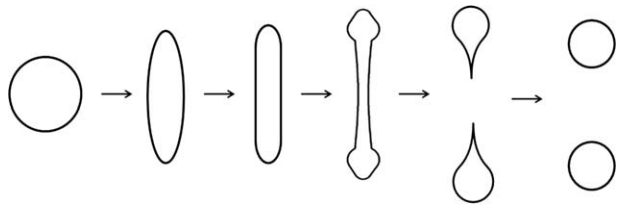

Figure 9. Diagrammatic sketch of deformation and breakup of droplet as a result of the interplay between the electrical force, surface tension and viscous force.

sophericity may be that large droplets are easier to deform under the impact into the coagulation bath.

Loscertales[45] has proposed an equation to describe the relationship between D_{av} and flow rate, which go as Eq. (1),

$$D_{av} = k(Q \cdot \varepsilon/\sigma)^{\frac{1}{3}} \quad (1)$$

where σ is surface tension, Q is flow rate, ε is dielectric constant, k is constant. In this work, D_{av} and Q was linearly fitted using Eq. (1), as shown in Figure 10. The calculated linear correlation coefficient (R^2) reaches to 0.9905. The good linear correlation between D_{av} and $Q^{1/3}$ gives the evidence that the particle size of RCM can be tuned by flow rate.

CONCLUSIONS

This article has shown that electrospraying can be used as a tool for the fabrication of RCM with desired sizes and architectures. The particle size and shape of RCM, which is mainly dependent on the interplay among the electrical force, surface tension, and viscous force, can be controlled by the manipulation of voltage, electrode spacing, solution system, concentration, DP, and flow rate. Generally, increasing electrical force and reducing surface tension and viscosity force lead to the decrease in particle size. Besides micorspheres, elongated spheres, tear-shaped, wedge-shaped, and banding-shaped particles are also created, especially by changing the viscosity. Owing to the controllability, uniformity, porosity, and "green" characteristic, RCM via electrospraying have potential applications in some fields such as chromatogram, water treatment, biomedicine and so forth.

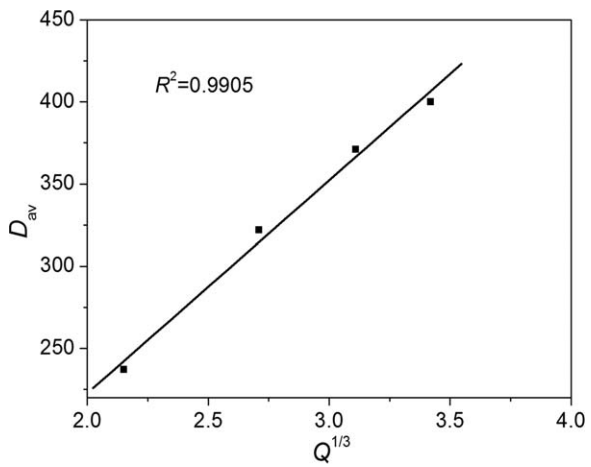

Figure 10. Particle size of RCM as a function of flow rate.

ACKNOWLEDGMENTS

The support of this work by the National Natural Science Foundation of China (No.31200453, No. 31300483) the Priority Academic Program Development of Jiangsu Higher Education Institutions (PAPD) and Jiangsu Provincial Government Scholarship for Overseas Studies is gratefully acknowledged.

REFERENCES

1. Nishiyama, Y.; Langan, P.; Chanzy, H. *J. Am. Chem. Soc.* **2002**, *124*, 9074.
2. Nishio, Y. *Adv. Polym. Sci.* **2006**, *205*, 97.
3. Luo, X.; Zhang, L. *J. Chromatogr. A* **2010**, *1217*, 5922.
4. Zhang, Y.; Xu, L.; Zhao, L.; Peng, J.; Li, C.; Li, J.; Zhai, M. *Carbohydr. Polym.* **2012**, 931.
5. Thümmler, K.; Fischer, S.; Feldner, A.; Weber, V.; Ettenauer, M.; Loth, F.; Falkenhagen, D. *Cellulose* **2011**, *18*, 135.
6. Luo, X.; Zhang, L. *Biomacromolecules* **2010**, *11*, 2896.
7. Thakare, M.; Israel, B.; Garner, S. T.; Ahmed, H.; Garner, P.; Elder, D.; Price, J. C.; Capomacchia, A. C. *Pharm. Dev. Technol.* **2013**, *18*, 1213.
8. Brent, S. M.; Kalpana, D.; Peter, W. N.; Antonia, K.; Simeon, D. S. *J. Agric. Food Chem.* **2011**, *59*, 13277.
9. Peng, B.; van der Wee, E.; Imhof, A.; van Blaaderen, A. *Langmuir* **2012**, *28*, 6776.
10. Song, J. S.; Tronc, F.; Winnik, M. A. *Polymer* **2006**, *47*, 817.
11. Guo, X.; Du, Y.; Chen, F.; Park, H.-S.; Xie, Y. *J. Colloid Interface Sci.* **2007**, *314*, 427.
12. Gericke, M.; Liebert, T.; Heinze, T. *Macromol. Biosci.* **2009**, *9*, 343.
13. Gharsallaoui, A.; Roudaut, G.; Chambin, O.; Voilley, A.; Saurel, R. *Food Res. Int.* **2007**, *40*, 1107.
14. I Ré, M. *Dry. Technol.* **1998**, *16*, 1195.
15. Hayati, I.; Bailey, A. I.; Tadros, Th. F. *J. Colloid Interface Sci.* **1987**, *117*, 205; 222.
16. Bailey, A. G. Elecrostatic Spraying of Liquids; Wiley: New York, **1988**.
17. van Honschoten, J. W.; Brunets, N.; Tas, N. R. *Chem. Soc. Rev.* **2010**, *39*, 1096.
18. Papadopoulou, S. K.; Tsioptsias, C.; Pavlou, A.; Kaderides, K.; Sotiriou, S.; Panayiotou, C. *Colloids Surf. A: Physicochem. Eng. Aspects* **2011**, *387*, 71.
19. Sun, L.; Yu, X.; Sun, M.; Wang, H.; Xu, S.; Dixon, J. D.; Wang, Y. A.; Li, Y.; Yang, Q.; Xu, X. *J. Colloid Interface Sci.* **2011**, *358*, 73.
20. Yu, D.G.; Yang, J. H.; Wang, X.; Tian F. *Nanotechnology* **2012**, *23*, 105606.
21. Yu, D. G.; Williams, G. R.; Yang, J. H.; Wang, X.; Yang, J. M.; Li, X. Y. *J. Mater. Chem.* **2011**, *21*, 15957.
22. Huang, L. Y.; Yu, D. G.; Christopher, B. W.; Zhu, L. M. *J. Mater. Sci.* **2012**, *47*, 1372.
23. Xie, J.; Marijnissen, J. C. M.; Wang, C.-H. *Biomaterials* **2006**, *27*, 3321.

24. Li, W., Yu, D. G.; Chen, K.; Wang, G.; Williams, G. R. *Mater. Lett.* **2013**, *93*, 125.
25. Kim, C.-W.; Kim, D.-S.; Kang, S.-Y.; Marquez, M.; Joo, Y. L. *Polymer* **2006**, *47*, 5097.
26. Frenot, A.; Henriksson, M. W.; Walkenstrom, P. *J. Appl. Polym. Sci.* **2007**, *103*, 1473.
27. Viswanathan, G.; Murugesan, S.; Pushparaj, V.; Nalamasu, O.; Ajayan, P. M.; Linhardt, R. J. *Biomacromolecules* **2006**, *7*, 415.
28. Frey, M. W.; Joo, Y.; Kim, C. *Abstr. Am. Chem. Soc.* **2003**, *226*, 404.
29. Cai, J.; Zhang, L.; Liu, S.; Liu, Y.; Xu, X.; Chen, X.; Chu, B.; Guo, X.; Xu, J.; Cheng, H.; Han, C. C.; Kuga, S. *Macromolecules* **2008**, *41*, 9345.
30. Qi, H.; Chang, C.; Zhang, L. *Green Chem.* **2009**, *11*, 177.
31. Langan, P.; Nishiyama, Y.; Chanzys, H. *J. Am. Chem. Soc.* **1999**, *121*, 9940.
32. Paavo, M.; Manu, L.; Kari, R. *Carbohydr. Polym.* **2007**, *68*, 35.
33. Jaworek, A.; Sobczyk, A. T. *J. Electrostatics* **2008**, *66*, 197.
34. Babak, V. H.; Behnam, S.; Mehdi, R. C.; Esmaeil, E. *Colloids Surf A: Physicochem. Eng. Aspects* **2012**, *401*, 17.
35. Elke, S.; Himanshu, D.; Lev, B.; Gregory, C. R.; Hatton, T. A. *Langmuir* **2011**, *27*, 6683.
36. Dabora, E. K. *Rev. Sci. Instrum.* **1967**, *38*, 502.
37. Loscertales, G. I.; Barrero, A.; Guerrero, I.; Cortijo, R.; Marquez, M.; Gañán-Calvo, A. M. *Science* **2002**, *295*, 1695.
38. Zheng, J.; He, A.; Li, J.; Xu J.; Han, C.-C. *Polymer* **2006**, *47*, 7095.
39. Smith, D. P. H. *IEEE Trans. Ind. Appl.* **1986**, *22*, 527.
40. Son, W. K.; Youk, J. H.; Lee T. S., Park W. H. *Polymer* **2004**, *45*, 2959.
41. Qi, H. S.; Sui, X. F.; Yuan, J. Y.; Wei, Y.; Zhang, L. N. *Macromol. Mater. Eng.* **2010**, *295*, 695.
42. Thompson, C. J.; Chase, G. G.; Yarin, A. L.; Reneker, D. H. *Polymer* **2007**, *48*, 6913.
43. Rayleigh, L. *Philos. Mag.* **1882**, *14*, 184.
44. Taylor, G. *Proc. Roy. Soc. London* **1964**, *A280*, 383.
45. Cara, J. Y.; Laura, A. P.; Penny, J. M. *Biotechnol. Bioeng.* **2012**, *109*, 1561.